A water resistance magnetic graphene-anchored zeolitic imidazolate framework for efficient adsorption and removal of residual tetracyclines in wastewater

Zelan Wang, XiaoYan Chen, Zhe Meng, Mengxin Zhao, Haijuan Zhan and Wanyi Liu

ABSTRACT

Water-resistant magnetic graphene-anchored zeolite imidazolate (Fe_3O_4/ZIF-8-G) composite materials with the largest surface area are formed by directly growing a hydrophobic ZIF-8 skeleton onto a graphene support through self-assembly in methanol. Fe_3O_4/ZIF-8-G hybrid composite has water resistance and super strong adsorption capacity, and is used as an effective adsorbent for adsorption and removal of residual tetracycline in wastewater. The morphologies and structure, as well as water resistance of Fe_3O_4/ZIF-8-G, were characterized using Fourier transform infrared spectroscopy (FT-IR), X-ray diffraction (XRD), scanning electron microscopy (SEM), transmission electron microscopy (TEM), thermogravimetry analysis (TGA), N_2 adsorption and pH_{PZC}. The adsorption for tetracycline (TC), oxytetracycline (OTC) and chlortetracycline (CTC) followed pseudo-second-order kinetics and fitted the Freundlich adsorption model with the simultaneous adsorption capacity for TC (382.58 mg g^{-1}), OTC (565.94 mg g^{-1}) and CTC (608.06 mg g^{-1}) at pH 5–6 for 10 h. These were much higher than previously reported results for the removal of tetracycline from aqueous solutions. The used Fe_3O_4/ZIF-8-G could be effectively reused and recycled at least five times without significant loss of adsorption capacity. The hydrophobic and π-π interaction between the aromatic rings of TCs and the aromatic imidazole rings of the ZIF-8-G framework were the main adsorption mechanism on the surface of Fe_3O_4/ZIF-8-G. Constructing a hydrophobic surface of ZIF-8/G framework resulted in a reduction of the hydrophilic sites of the surface. This can improve stability and selective adsorption of ZIF-8-G framework. In addition, the results show no significant difference in the adsorption kinetics and adsorption capacity of Fe_3O_4/ZIF-8-G for TC, OTC and CTC in pure water and wastewater.

Key words | adsorption, Fe_3O_4/ZIF-8-G, tetracyclines, wastewater, water resistance

Zelan Wang†
XiaoYan Chen†
Zhe Meng (corresponding author)
Mengxin Zhao
Haijuan Zhan
Wanyi Liu
State Key Laboratory of High-Efficiency Utilization of Coal and Green Chemical Engineering, College of Chemistry and Chemical Engineering,
Ningxia University,
Yinchuan 750021,
China
E-mail: *meng_z@nxu.edu.cn*

†These authors contributed equally.

HIGHLIGHTS

- The synergistic effect between hybrid ZIF-8/G and magnetic separation significantly enhanced adsorption capacity of tetracyclines onto Fe_3O_4-ZIF-8/G.
- The π-π stacking interaction between the aromatic rings of the tetracyclines and the aromatic imizole rings of the ZIF-8 was responsible for the efficient adsorption.
- The large adsorption capacity, good selectivity and excellent reusability create potential for Fe_3O_4-ZIF-8/G to be effective removing TCs from influent and effluent of wastewater treatment systems.

doi: 10.2166/wst.2020.283

GRAPHICAL ABSTRACT

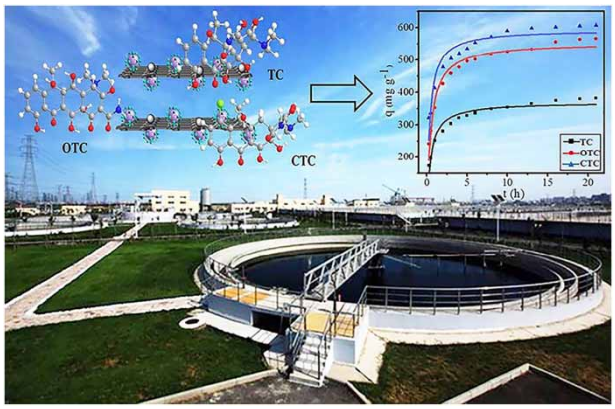

INTRODUCTION

The pharmaceuticals, especially antibiotics, are frequently detected in surface water, ground water, as well as in effluent of wastewater treatment systems (Ahmadi *et al.* 2017; Zheng *et al.* 2017). As the average daily antibiotic dose in China is almost five times that of Americans or Europeans, effective coping techniques for removing antibiotics in Chinese waters have become more urgent (Ying *et al.* 2016). Among many antibiotics, tetracycline derivatives (TCs) mainly including tetracycline (TC), oxytetracycline (OTC) and chlortetracycline (CTC), are widely used to treat animal diseases and promote the growth of aquaculture and animal husbandry. Thus, most TCs are excreted through urine and feces, and are eventually introduced into wastewater (Senta *et al.* 2013; Wang *et al.* 2018), especially actinomycete or pathogenic bioaccumulation in contaminated environmental water (Senta *et al.* 2013; Zhang *et al.* 2015; Ying *et al.* 2016; Wang *et al.* 2018; Islam & Gilbride 2019). It is necessary to research and develop appropriate technologies to remove the antibiotics from water. Currently, adsorption, biodegradation, chemical oxidation, photochemical degradation and electrochemistry technologies have been used for the removal and degradation of TCs (Lee *et al.* 2006; Shi *et al.* 2007; Mahanta *et al.* 2008; Kulkarni *et al.* 2014; Guan *et al.* 2017). Comparing these methods, the removal of TCs via adsorbents has become more popular due to its relatively low cost, being harmless to the environment and simple and convenient, with the iteration of adsorption material and the diversified discovery of material design. At present, some of the materials, including graphene-based materials (Yu *et al.* 2016), biomass-based materials such as chitosan (Ahamad *et al.* 2019), biochar (Zeng *et al.* 2019) and nanoadsorbents (Tombuloglu *et al.* 2018), have been receiving more attention. Among them, carbon-based materials, especially graphene, have been summarized in the previous review (Yu *et al.* 2016). The specific surface area is important in adsorption. However, the application of graphene-based materials as adsorbents for the adsorption of TCs is still far from sufficient.

Recently, metal-organic frameworks (MOFs) have been widely used to capture organic pollutants in wastewater (Furukawa *et al.* 2013; Peng *et al.* 2017). The advantage of MOFs as adsorbents for TCs has been evident; for instance, the adsorptive removal of TC by MOFs or MOF-based material for TC on MOF-5 (Mirsoleimani-azizi *et al.* 2018), CuCo/MIL-101 (Jin *et al.* 2019), H-UiO-66s (Yang *et al.* 2019), etc. However, the stability and adsorption performances of these MOF materials in water are very poor. According to the experimental and theoretical work of previous study (Sava *et al.* 2013; Chibani *et al.* 2018), the hydrogen bonds play an important role in the different MOFs structures on the adsorption behavior of target compounds. Perhaps the most important problem is that a large number of hydrophilic sites in the framework of MOFs are readily occupied by water molecules or a metal cluster is hydrolyzed.

Zeolitic imidazolate frameworks (ZIFs), as a branch of MOFs, have permanent porosity and some of the highest chemical and thermal stability among MOF materials. Moreover, ZIF materials can possess an inherently hydrophobic framework (Venna *et al.* 2010; Zhang *et al.* 2013).

This makes them ideal candidates, which have attracted great attention in various applications (Xu *et al.* 2010; Sumida *et al.* 2012; Yoon *et al.* 2012; Zhao *et al.* 2014), especially towards dye and organic pollutants in environmental wastewater such as 1H-benzotriazole and 5-tolyltriazole on ZIF-8 (Jiang *et al.* 2013), Cu^{2+} on ZIF-8 (Zhang *et al.* 2016), sulfamethoxazole on ZIF-8 (Ahmed *et al.* 2017) and ciprofloxacin on ZIF-8 (Li *et al.* 2017a), as well as ZIF-8 for the extraction of trace TC (Wu *et al.* 2015) and Fe_3O_4@ZIF-8 composites for the extraction of trace TC (Liu *et al.* 2017). However, the drawbacks also are the low adsorption capacities. According to the theoretical study previously reported (Chibani *et al.* 2018), ZIF-8 is hydrophobic, but its own zeolite framework structure, of a three-dimensional network composed of supercages (diameter 2.3–7.4 Å), is too sensitive to water. To solve these problems, constructing a water resistance surface of MOFs and removing the hydrophilic sites on the surface is one of the effective strategies to improve its framework stability and adsorption performance.

Recent studies have tried to address the above challenges. From the previous study, the oxygen functionalities of GO (hydroxyl, carboxyl, epoxy, ketone) are able to coordinate to the metallic centers of the MOFs, and thus allow the growth of crystals onto the graphene layers. This gives better adsorption ability to the composite compared with the virgin MOF alone (Petit & Bandosz 2011; Ahmed & Jhung 2014; Peng *et al.* 2018). However, GO has a hydrophilic character, resulting in the easy dispersion of GO in water, which seriously affects the stability of hybrid composites. Hydrophobic G is more advantageous than GO, because the green preparation of graphene by directly exfoliating crystal graphite powder in the water-alcohol mixture was facile, green, low cost, and potentially large-scale (Yi *et al.* 2012). Considering with ZIF-8 nanoparticles directly coupled to the surface of the G by self-assembly that special ZIF-8-G materials show ideal hydrophobic properties. The hydrophobicity of the ZIF-8 structure offers the potential convenience of achieving good interfacial interaction between ZIF-8 and G in hybrid mixed matrix systems, thereby also making ZIF-8-G a promising material for the efficient adsorption and removal of residual tetracyclines in wastewater.

In this study, a water resistant magnetic graphene-anchored zeolitic imidazolate hybrid composite (Fe_3O_4/ZIF-8-G) was synthesized as a novel adsorbent for the adsorption and removal of TCs at high concentrations (200 mg L^{-1}) from wastewater. In ternary composites, the sheet hydrophobic G is a carrier of well-defined ZIF-8 nanoparticles of ~30 nm, which were well dispersed and fully confined on the G sheet. Magnetic Fe_3O_4 particles of 0.4 μm were dispersed on the surface of ZIF-8-G, and also act as a magnetic separator. This novel synthesized adsorbent and its absorbability for TCs at high concentration (200 mg L^{-1}), has been first systematically studied through the batch adsorption experiments, combining the high-performance liquid chromatography-mass spectrometry methods. The adsorption kinetics, thermodynamics, and regeneration of Fe_3O_4/ZIF-8-G as an adsorbent for simultaneous removal of TC, OTC and CTC from the effluent of a wastewater treatment system were systematically investigated through batch adsorption experiments.

MATERIALS AND METHODS

Chemicals and materials

TC ($C_{22}H_{24}N_2O_8$·HCl, 480.8955 g mol^{-1}), OTC ($C_{22}H_{24}N_2O_9$·2HCl, 517.3564 g mol^{-1}) and CTC hydrochloride salt ($C_{22}H_{23}ClN_2O_8$·HCl, 515.3406 g mol^{-1}), with a purity of 99.5%, were obtained from Macklin (Shanghai, China). Methanol and acetic acid (HOAc) of HPLC grade were obtained from Fisher (Pittsburgh, USA). Zinc nitrate hexahydrate ($Zn(NO_3)_2$·$6H_2O$, 99.99%), 2-methylimidazole ($C_4H_6N_2$, 98%), and commercial graphite powder with D50 < 600 nm and a purity of 99.9% were obtained from Aladdin (Shanghai, China). Ferric chloride hexahydrate ($FeCl_3$·$6H_2O$), anhydrous sodium acetate (NaAc), macrogol 2000 (PEG-2000) and ethylene glycol (EG) of analytical grade were obtained from Damao (Tianjin, China). Mixed stock standard solution of TCs at concentrations of 1,000 mg L^{-1} of each compound was prepared with double distilled water. The stock and working standard solutions were stored in a refrigerator at 4 °C. All solutions were prepared with ultrapure water using a Milli-Q system (Millipore, Billerica, USA). The wastewater samples (including effluent, influent, aeration water, pH 5.5–6.5 at 20 °C) were collected from wastewater treatment plant (Xixia District, Yinchuan, Ningxia).

Preparation of adsorbent

The Fe_3O_4 particles were synthesized via the chemical co-precipitation hydrothermal method according to the literature (Li *et al.* 2005), and detailed in the supplementary information. The graphene was prepared using the green

preparation method by liquid-phase exfoliation of graphite in a mixture of water and alcohol (Yi *et al.* 2012), as detailed in the supplementary information. X-ray diffraction (XRD) analysis of an exfoliated graphite sheet is shown in Figure S1 (supplementary information). A very weak peak was presented for the exfoliated graphite sheet at 2θ-26.6°, corresponding to the (002) planes compared with the graphite powder. This may be attributed to an unchanged layer-to-layer distance from graphite. The above-mentioned very thin flakes or graphene layers demonstrated a high degree of exfoliation.

Secondly, the hybrid composites ZIF-8-G were synthesized by ZIF-8 crystals directionally growing on the G layer with mechanical stirring in methanol at room temperature. Compared with the case of previous studies, the yield of ZIF-8 was increased by 30% with time reduction (Peng *et al.* 2018). Briefly, 0.410 g of Zn $(NO_3)_2{\cdot}6H_2O$ and 20 mg of G were dispersed in 100 mL of anhydrous methanol and sonicated for 4 h. 0.744 g of 2-methylimidazole was added to the solution with mechanical stirring at room temperature for 6 h. The resulting precipitate was collected by centrifugation at 4,000 rpm for 15 min, then washed three times with 40 mL of methanol, and finally freeze-dried for 12 h to obtain the ZIF-8-G composite powder. Subsequently, Fe_3O_4 particles were loaded by electrostatic action. 15 mg of prepared Fe_3O_4 was dispersed in 30 mL of anhydrous methanol by ultrasound for 30 min. Then, 25 mg of ZIF-8-G was added to the solution with continuous mechanical stirring at room temperature for 15 h. The resulting precipitates were collected with a magnet, and washed several times with methanol. Finally, they were freeze-dried to obtain the sample Fe_3O_4/ZIF-8-G composite materials.

Characterization studies

The crystallinity of the prepared samples was characterized by XRD (Bruker-D8-ADVANCE A25 X-ray diffractometer) with Cu Kα radiation and a scan rate of 5° min^{-1} ranging from 3 to 85°. The microscopic morphology of the samples was observed by transmission electron microscope (TEM, FEI Talos 200S) and scanning electron microscope (SEM, Hitachi SU8020). The Fourier transform infrared (FT-IR) spectra were recorded on a Shimadzu IRAffinity-1S, and data were collected in the range of 400–4,000 cm^{-1}. Thermogravimetry analysis (TGA) was carried out using a Setaram setsys 16 instrument. Pore volume and Brunauer–Emmett–Teller (BET) surface area measurements of the synthesized materials were analyzed through N_2 adsorption/desorption isotherms with a micromeritics surface area and porosity analyser (ASAP2010-M).

Analytical method

A LC-MS-2010EV high performance liquid chromatograph (HPLC) equipped with mass spectrometry (MS) was applied to the analysis of TCs residues (Shimadzu, Japan). The separation of TCs antibiotic was performed on a Kromasil-C_{18} (100 mm × 4.6 mm, 3.5 μm) column. The mobile phases A and B were H_2O with 0.1% HOAc and methanol, respectively. Gradient elution conditions were as follows: 0.1–3 min, 30%–40% B; 4–30 min, 40%–70% B; 31–35 min, 70% B; 36–40 min, 70%–30% B. The flow rate was 0.35 mL min^{-1}. The temperature of the column was set at 35 °C. Sample injection volume was 20 μL. The mass spectrometric detection was performed in positive ion mode. Quantitative analysis was in selective ion monitoring (SIM) mode. The quantification ion for the target analytes is m/z 445.44 (TC), m/z 461.44 (OTC), m/z 479.88 (CTC).

Linearity was studied from matrix-matched calibration with effluent spiking samples at the eight concentration levels (0.02, 0.05, 0.10, 0.50, 2.00, 5.00, 10, 20 μg mL^{-1}) for HPLC-MS analysis. The calibration curves showed good linearity with a correlation coefficient (R^2) greater than 0.9985. The limits of detection (LOD) were 3.8–7.5 ng mL^{-1}, and the limits of quantification (LOQ) were 12.5–25 ng mL^{-1}. We can calculate antibiotic TCs as signal-to-noise ratio (S/N) 3:1 and 10:1, respectively.

Adsorption experiments

Adsorption experiments of Fe_3O_4/ZIF-8-G

The concentrations of TCs mixture in all batch adsorption experiments were obtained by diluting the individual stock solution. 20 mg of adsorbent was added to a 150 mL conical flask containing 100 mL of the TCs mixture. The conical flasks were placed in a 308 K thermostatic water bath with shaking speed of 100 rpm for batch adsorption experiments. Sampling was carried out by isolating the sorbent using magnets, and supernatant was filtered by using 0.22 μm nylon filters. Finally, the sample was analyzed by HPLC-MS.

We investigated TCs mixture of 50 mg L^{-1}, and then discussed the pH (initial pH from 3 to 11) adjusted with 0.1 M HCl or NaOH with a pH meter, adsorbent dosage (5 mg, 10 mg, 20 mg, 30 mg and 40 mg), initial antibiotic concentration (5 mg L^{-1}, 10 mg L^{-1} and 50 mg L^{-1}, 100 mg L^{-1}

and 200 mg L^{-1}), contact time (10 min–20 h), and adsorption temperature (298 K, 308 K, 318 K and 328 K). The confirmation and measurement of TCs in mixed solution were carried out using the HPLC-MS method. All experiments were performed in triplicate to obtain the average result for data analysis. The removal efficiency of each antibiotic was calculated using Equation (1). The adsorption capacity at equilibrium (q_e, mg g^{-1}) and time t (q_t, mg g^{-1}) were calculated using Equations (2) and (3), respectively (Li *et al.* 2017b).

$$\text{Removal efficiency}: \text{e} = \frac{C_0 - C_e}{C_0} \tag{1}$$

$$q_e = (C_0 - C_e) \times \frac{V}{W} \tag{2}$$

$$q_t = (C_0 - C_t) \times \frac{V}{W} \tag{3}$$

where C_0, C_e and C_t are concentrations (mg L^{-1}) of TCs solution at the initial time, equilibrium and time t (min), respectively. V is the volume of the solution (L). w is the mass of the adsorbent (g).

Adsorption kinetic of Fe_3O_4/ZIF-8-G

Adsorption kinetic data were obtained by single batch experiments for the antibiotic mixture related to three initial concentrations of 50, 100, 200 mg L^{-1}. The constant test was carried out with adsorbent weight of 20 mg (0.2 mg mL^{-1}), pH of 5–6, temperature at 308 K and a contact time of 0.25–20 h.

The three most common adsorption kinetic models are the pseudo-first-order model, the pseudo-second order model and the intra-particle diffusion model. They are usually applied to interpret the experimental results (Ho & McKay 1999; Özcan *et al.* 2005; Ho 2006).

The pseudo-first-order model is expressed as follows:

$$\ln (q_e - q_t) = \ln q_e - k_1 t \tag{4}$$

The pseudo-second-order model is expressed as follows:

$$\frac{\text{t}}{q_t} = \frac{1}{k_2 q_e^2} + \frac{t}{q_e} \tag{5}$$

The intra-particle diffusion model is expressed as follows:

$$q_t = k_3\, t^{1/2} + c \tag{6}$$

where q_e and q_t (mg g^{-1}) are the amounts of TCs adsorbed at the equilibrium and time t (min), respectively. k_1 (min^{-1}) is the first-order rate constant; k_2 (mg g^{-1} min^{-1}) is the second-order rate constant; k_3 (mg g^{-1}·$min^{-1/2}$) is the intra-particle diffusion rate constant. c (mg g^{-1}) is a constant about the thickness of the boundary layer.

Adsorption isotherms of Fe_3O_4/ZIF-8-G

Adsorption equilibrium data were obtained by single batch experiments for antibiotic mixture using the concentration variation method at three different temperatures (298 K, 308 K and 318 K). The experiments were carried out with the initial concentrations of 5, 10, 50, 100 and 200 mg L^{-1} for TCs, an adsorbent quantity of 20 mg, a pH of 5–6, and a contact time of 10 h. The equations of the Langmuir isotherm and Freundlich isotherm models are described as follows (Gupta *et al.* 2005; El Qada *et al.* 2008).

Langmuir isotherm:

$$q_e = \frac{q_{\max} K_L C_e}{1 + K_L C_e} \tag{7}$$

Freundlich isotherm:

$$q_e = K_F C_e^{1/n} \tag{8}$$

where q_e (mg g^{-1}) is the adsorption capacity of TCs at equilibrium. $q_{\max}$ (mg g^{-1}) is the maximum adsorption capacity of TCs. K_L is the Langmuir adsorption constant at equilibrium. C_e (mg L^{-1}) is the solution concentration at equilibrium. K_F is the Freundlich constant. $1/n$ is the adsorption intensity.

Adsorption thermodynamics of Fe_3O_4/ZIF-8-G

During the adsorption process, both energy and entropy factors determine what processes will occur spontaneously. Thermodynamic parameters of TCs removal by Fe_3O_4/ZIF-8-G were tested by adsorption at three different temperatures using the following Equations (9) and (10). Gibbs free energy change (ΔG), enthalpy change (ΔH) and entropy change (ΔS) can be calculated by the Van't Hoff equations as follows (Gupta *et al.* 2005; El Qada *et al.* 2008):

$$\Delta G = -RT \ln K \tag{9}$$

$$\ln K = \frac{\Delta H}{-RT} + \frac{\Delta S}{R} \tag{10}$$

Recycle experiments

The feasibility of recycling adsorbent Fe_3O_4/ZIF-8-G affects its application. In this work, the collected adsorbent was sonicated in 0.1% acetate-acetonitrile solution for 1 h to be completely desorbed. Then, the regenerated adsorbent was separated from solution using magnets, washed with water and dried. Finally, it was used for the next adsorption experiment.

RESULTS AND DISCUSSION

Characterization of the prepared adsorbent Fe_3O_4/ZIF-8-G

The prepared samples were characterized by XRD, FTIR, TGA, SEM, TEM, N_2 adsorption and Zeta potential experiments. As shown in Figure 1, the typical diffraction peaks of the samples appeared at $2\theta = 7.3°$ (011), 10.4° (002), 12.7° (112), 14.7° (022), 16.4° (013), 18.0° (222), 24.5° (233) and 26.7° (134), which is in good agreement with that of ZIF-8 phase in previous studies (Wu *et al.* 2015; Liu *et al.* 2017). However, the relative intensities of the main peak for ZIF-8, corresponding to $2\theta = 7.3°$ (011), was quantified to determine the relative crystallinity of the ZIF-8 phase. The (011) peak on ZIF-8-G is slightly higher than that of the (011) peak on ZIF-8. Therefore, ZIF-8 can grow directly on G. This leads to perpendicular alignment of the ZIF-8 polyhedron with high crystallinity, which helps prevent restacking of the ZIF-8 nanoparticles structure. According to the standard diffractogram of Fe_3O_4 (JCPDS: 79-0418), the intense reflection of Fe_3O_4 appeared at $2\theta =$ 30.2°, 35.4°, 43.1°, 53.7°, 57.0°, 62.8°. However, no sign of G is observed on this composite material. Due to the high degree of exfoliation, this may be a graphene layer, which is consistent with literature reports (Yi *et al.* 2012). In addition, the stability of the Fe_3O_4/ZIF-8-G composites was investigated by sonication processing in aqueous solution with different pH values (pH = 4, 7, 10). The intensities decreased slightly for the typical diffraction peaks (Figure 1). There was no significant change in the peak position of the sample. Hence, Fe_3O_4/ZIF-8-G exhibited excellent water resistance, which contributes to hybridization of hydrophobic ZIF-8 and G.

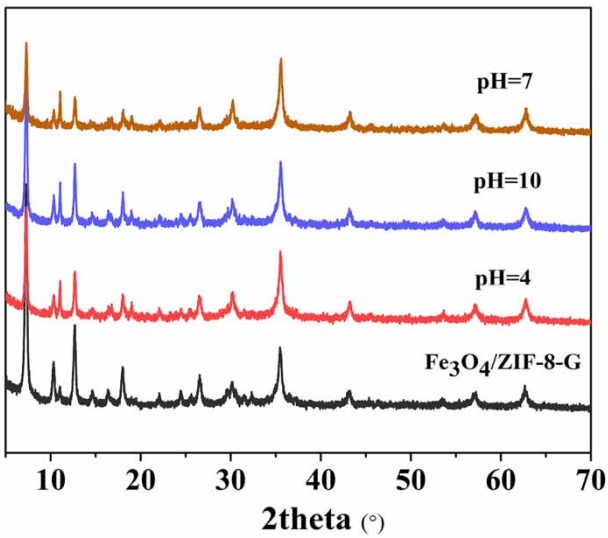

Figure 1 | XRD spectra of Fe_3O_4/ZIF-8-G in different pH aqueous solution with sonication for 1 h.

The TEM images of the samples are shown in Figure 2. ZIF-8 crystals are homodisperse with a sharp angular surface (Figure 2(a) and 2(b)) and have a clear dodecahedral shape with a narrow size distribution of 30–40 nm (Figure 2(c)). The Fe_3O_4 particles are homodisperse with spherical size distribution around 400 nm (Figure 2(a)). For G, a very dense and disordered arrangement of graphene layer is observed (Figure 2(b) and 2(c)). The EDS patterns of Fe_3O_4/ZIF-8-G composite are shown in Figure 2(d). The yellow, purple, brown, lake blue and blue dots represent the EDS patterns of Fe, Zn, C, N and O elements, respectively, which were uniformly distributed on the surface of the Fe_3O_4/ZIF-8-G composite in Figure S2 (supplementary information). In sum, the Fe_3O_4/ZIF-8-G composite was successfully prepared.

SEM images are presented in Figure 3. The relative crystallinity of ZIF-8 is more complete, which is in good agreement with the previous studies (Wu *et al.* 2015; Liu *et al.* 2017). The homodisperse ZIF-8 nanoparticles growing on the surface of a folded G layer show a close arrangement (Figure 3(a)). However, the distribution of ZIF-8 cannot be observed on the surface of spherical Fe_3O_4 (Figure 3(b)). The SEM image further proves that the strong anchoring of ZIF-8 on the surface of G contributes to the interaction between π conjugated structure of G and 2-methylimidazole of ZIF-8. Thus, the hydrophobic ZIF-8-G framework is beneficial to the stability and immobility of composite materials used as an adsorbent with ultra-high adsorption capacity.

FT-IR spectra of Fe_3O_4/ZIF-8-G before and after the simultaneous adsorption of TCs and ZIF-8-G were recorded. As shown in Figure 4, FT-IR of the Fe_3O_4/ZIF-8-G composite is mainly attributed to Fe_3O_4, ZIF-8. Among them, the stretching peak at 422 cm^{-1} belongs to the Zn-N stretching

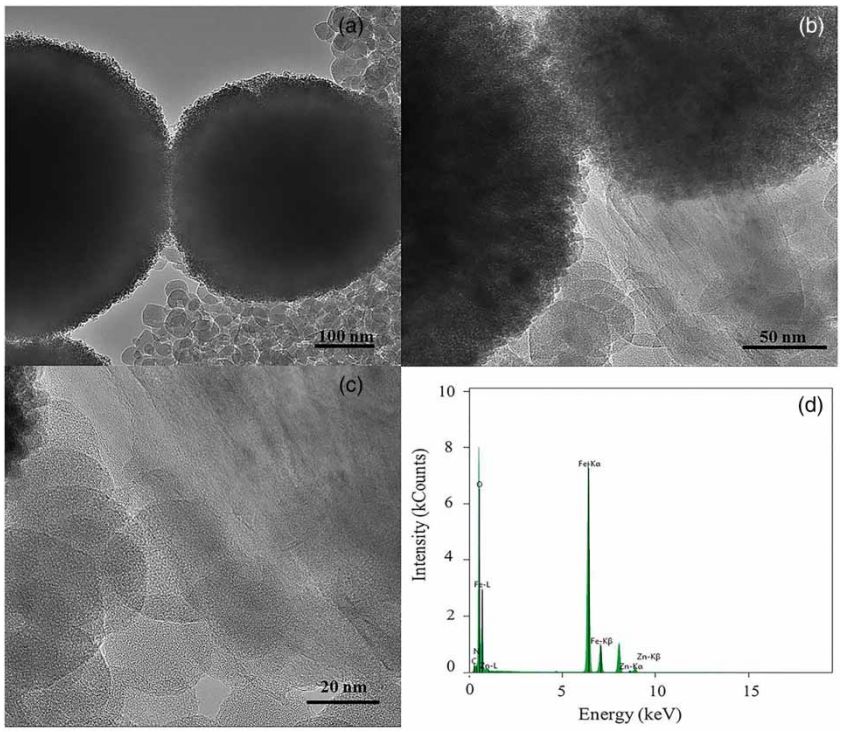

Figure 2 | TEM images and EDS patterns of Fe_3O_4/ZIF-8-G.

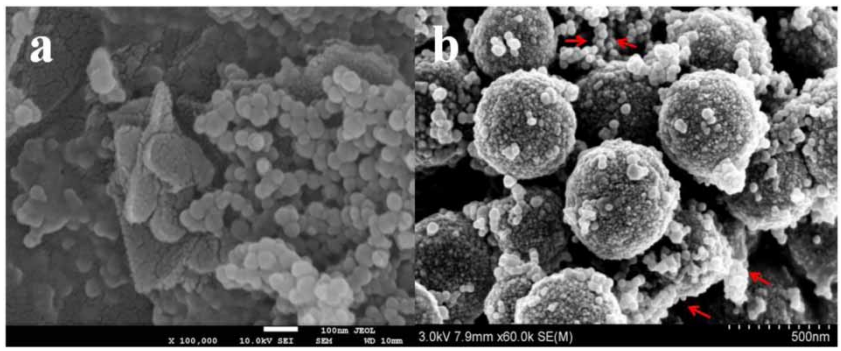

Figure 3 | SEM images of (a) ZIF-8-G and (b) Fe_3O_4/ZIF-8-G.

vibration, and some characteristic peaks in the range between 1,584 and 685 cm^{-1} belong to the stretching vibrations of the imidazole ring, which all can be attributed to the functional group of ZIF-8. This is in good agreement with previous studies (Wu *et al.* 2015; Liu *et al.* 2017). A broad peak in the range of 590 m^{-1} was attributed to the existence of Fe-O. After the absorption, a strong peak appearing at 1,580 cm^{-1} was obscured, which was attributed to the aromatic ring group of the adsorbed substance, further demonstrating that the TCs were adsorbed on Fe_3O_4/ZIF-8-G. More importantly, meaningless change of all characteristic peaks corresponding to synthesized ZIF-8 was significant after the absorption. This indicates that the structure of Fe_3O_4/ZIF-8-G remained stable in the adsorption process. In other words, the special structure of the composite effectively overcomes the intrinsic defects of poor water resistance of the MOF based materials reported (Mirsoleimani-azizi *et al.* 2018; Jin *et al.* 2019; Yang *et al.* 2019). It is expected to become a new type of adsorbent for efficient water treatment.

N_2 adsorption and desorption isotherms of Fe_3O_4/ZIF-8-G were measured before and after the simultaneous

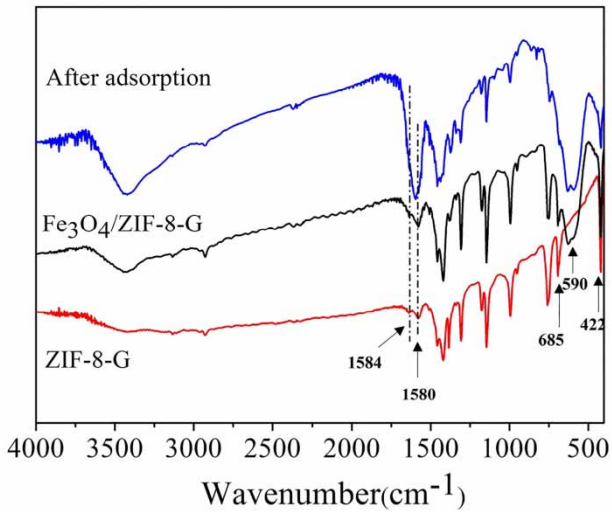

Figure 4 | FTIR of Fe_3O_4/ZIF-8-G before and after simultaneous adsorbing TCs.

adsorption of TCs. As shown in Figure S3, the isotherm of the Fe_3O_4/ZIF-8-G is of type IV as per IUPAC classification with type H4 hysteresis loop. The N_2 adsorption result showed the BET surface area of the prepared Fe_3O_4/ZIF-8-G was 492.4341 $m^2\,g^{-1}$ with pore size distribution of 4.0456 nm and a pore volume of 0.2117 $cm^3\,g^{-1}$. After the adsorption of TCs, the BET surface area of Fe_3O_4/ZIF-8-G was 253.0992 $m^2\,g^{-1}$ with pore diameter of 4.4789 nm and pore volume of 0.0980 $cm^3\,g^{-1}$. Results indicated that adsorption interaction of TCs onto Fe_3O_4/ZIF-8-G is likely to occur on the surface of the adsorbent compared with before and after the adsorption of TCs on Fe_3O_4/ZIF-8-G.

The thermal stability of the Fe_3O_4/ZIF-8-G composite was analyzed by TGA. Figure S4 shows weight losses of samples in the ranges of 33–104 °C and 268–622 °C. The initial weight loss could be attributed to the loss of guest molecules (water, methanol, or 2-methylimidazole). The rapid weight loss in the later range may be due to the collapse of the ZIF-8 framework. The TGA result further indicates that the main framework ZIF-8 in the prepared composite remained stable up to 600 °C.

Effect of pH on TCs adsorption

The pH value is related to the surface charge, which influences the adsorbate-adsorbent interaction. TCs molecules have three ionic states, including cationic species (pH < 3.3), zwitterionic species (3.3 < pH < 7.8) and anionic species (pH > 7.8). The zeta potential results show that the surface of Fe_3O_4/ZIF-8-G is positively charged with a pH = 3–10, which is consistent with previous studies (Wu *et al.* 2015; Liu *et al.* 2017; Peng *et al.* 2018). In this adsorption experiment, Fe_3O_4/ZIF-8-G composite (20 mg) was added into TCs water samples (100 mL) with the initial concentration of 50 mg L^{-1} and pH values ranging from 3.0 to 10.0 at 308 K. Figure 5 shows the effect of pH on removal efficiency. With the increase of the pH, the removal efficiency significantly increased (pH = 3–5), then leveled off (pH = 5–8), and finally decreased (pH = 8–10). When pH was in the range of 5–8, TCs became zwitterion molecules, and the surface charge of Fe_3O_4/ZIF-8-G remained positive, which caused weak electrostatic attraction. However, the adsorption efficiencies of TCs remained high, which demonstrated the hydrophobic and π-interaction between the aromatic rings of TCs and the aromatic imidazole rings of the ZIF-8-G framework. The results show the high potential of Fe_3O_4/ZIF-8-G at pH 5–6 for the adsorption and removal of TCs in aqueous solution. Considering the cage-filling mechanism, the characterized data about BET surface area and micropore area for Fe_3O_4/ZIF-8-G are summarized in Table 1. The specific surface area and porosity of Fe_3O_4/ZIF-8-G material were compared before adsorption, after adsorption, and after reusing 5 times. The specific surface area rapidly dropped from 492.4 to 253 $m^2{\cdot}g^{-1}$ with increasing adsorption capacity compared with before adsorption, but the porosity slightly decreased (85%–77%). Results further show that the occurrence of cage-filling for TCs was not consistent with the magnitude of Fe_3O_4/ZIF-8-G cage sizes, because the average pore size (~4.0 Å) of ZIF-8 was smaller than most TCs molecules (Peng *et al.* 2018). In

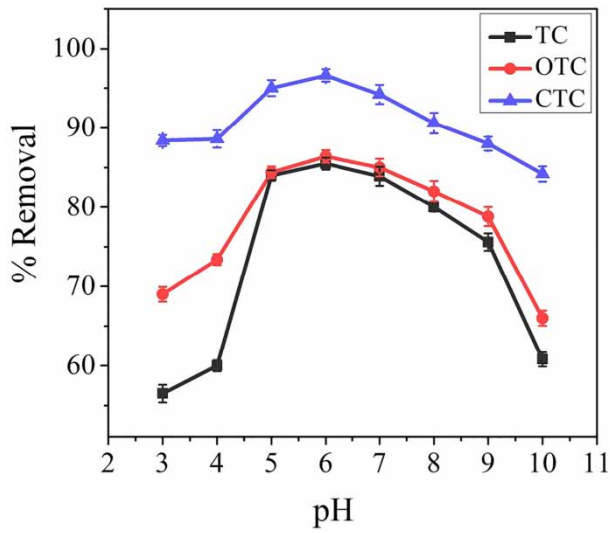

Figure 5 | Effect of solution pH on removal of TCs (C_0 = 50 mg L^{-1}, w = 20 mg, T = 308 K, t = 6 h).

Table 1 | Textural properties of Fe_3O_4/ZIF-8-G composites including surface areas and pore volumes

Fe_3O_4/ZIF − 8-G	BET ($m^2\ g^{-1}$)	Micropore area ($m^2\ g^{-1}$)	Micropore area/BET	Average pore size (nm)
Before adsorption	492.4341	417.6376	84.8%	4.0456
After adsorption	253.0992	194.2631	76.8%	4.4789
Recycled 5 times	184.5096	165.8775	89.9%	4.5677

other words, the small micropore size of ZIF-8 did not facilitate the incident of cage-filling.

Based on the above analysis, the results show that the electrostatic interaction was not the main mechanism involved in the efficient adsorption of TCs on Fe_3O_4/ZIF −8-G. The hydrophobic and π-π interaction between the aromatic rings of TCs, the aromatic imidazole rings of the ZIF-8-G framework, and the hydrogen bonding of -OH on the TCs to nitrogen atoms in the ZIF-8 framework were mainly responsible for the efficient adsorption (Figure 6).

Optimization of adsorption conditions

Several experimental parameters affecting the adsorption efficiency were investigated under the optimal pH range of 5–6, including the contact time (Figure S5), temperature (Figure S5), initial concentration (Figure S6) and adsorbent dose (Figure S7). The chromatographic peak area was carried out to assess the adsorption efficiency. All optimization batch experiments were described in detail in the supporting information. The following experimental conditions were found to give best results: 308 K for the optimal temperature; 20 mg for the optimal sorbent amount (0.2 mg mL^{-1}) far less than the reported 120 mg (1.2 mg mL^{-1}) in previous literature (Peng *et al.* 2018), the maximum adsorption equilibriums were reached within 10 h with an initial concentration less than 200 mg L^{-1}. However, at a high TCs concentration (200 mg L^{-1}), the efficiency of ZIF-8 decreased below 50% of the original value, while Fe_3O_4/ZIF-8-G still removed up to 90% within 10 h. This indicates that the composite material has better adsorption capacity than the original ZIF-8 alone.

Adsorption kinetics for TCs

The adsorption kinetics of TCs on Fe_3O_4/ZIF-8-G was investigated at three initial concentrations (50, 100 and 200 mg L^{-1}). The adsorption equilibrium of TCs was arrived

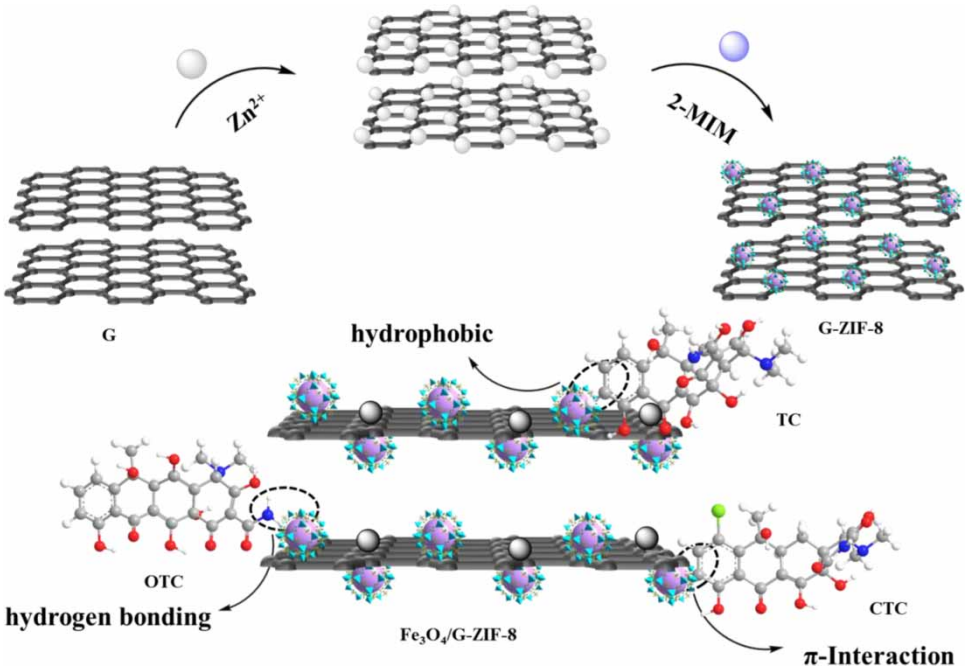

Figure 6 | Possible interactions between Fe_3O_4/ZIF-8-G and TCs including hydrophobic, π-interaction and hydrogen bonding.

at within 2 h at the initial concentration of 50 mg L^{-1}. The maximum adsorption equilibrium were controlled within 10 h at the initial concentration of less than 200 mg L^{-1}. Although the adsorption of TCs on Fe_3O_4/ZIF-8-G was time dependent, the adsorption capacities for TCs increased with the TCs initial concentration, and showed the high adsorption capacity of TCs at high concentrations. Comparing three types of classic quantitative dynamic models (Özcan *et al.* 2005; Ho 2006; El Qada *et al.* 2008), the experimental data were carried out and fitted by making the plot of q versus t (Figure 7, Figures S8 and S9). Some kinetic parameters are summarized in Table 2.

High correlation coefficients data ($R^2 > 0.9020$) were observed, and the calculated value of $q_{e(\mathrm{cal})}$ was in good agreement with the actual measured data $q_{e(\mathrm{exp})}$ (Table 2). Thus, the adsorption kinetics of TCs on Fe_3O_4/ZIF-8-G were much better fitted with the pseudo-second order kinetic model in Figure 7. With the initial concentration increased for TCs, K_2 rapid reduction indicated that chemisorption was significant in the rate-limiting step in the initial adsorption. However, for the intra-particle diffusion model in TCs on the Fe_3O_4-ZIF-8/G adsorption process (Figure S9), a good linear relationship ($R^2 > 0.8043$) is observed in Table 2. With the initial concentration increased for TCs, K_3 slowly increased, indicating that physical adsorption was significant in the rate-limiting step in the later adsorption.

Adsorption isotherms and thermodynamics for TCs

The adsorption isotherm models were studied at three different temperatures (298 K, 308 K, 318 K) in the concentration range of 5–200 mg L^{-1}. Langmuir and Freundlich isotherm models were conducive to the discussion of the adsorption mechanism (Gupta *et al.* 2005; El Qada *et al.* 2008). With the temperature increased from 298 K to 318 K, the maximum adsorption capacities were increased from 159.74 to 381.68 mg g^{-1} for TC, 198.81 to 892.86 mg g^{-1} for OTC

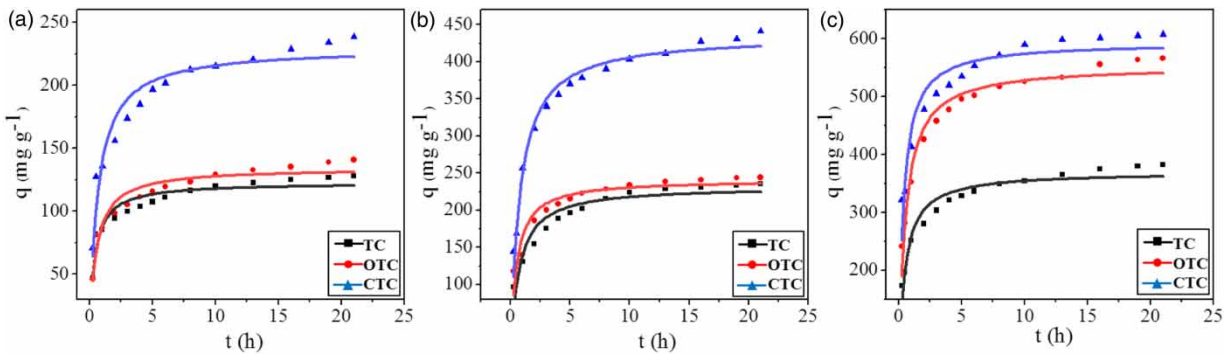

Figure 7 | Time-dependent adsorption of TCs and the plots of pseudo-second-order kinetics for the adsorption of TCs with different initial concentrations: (a) 50 mg L^{-1}, (b) 100 mg L^{-1}, (c) 200 mg L^{-1} under optimal adsorption conditions ($w = 20$ mg, pH = 5–6, $T = 308$ K).

Table 2 | The kinetic parameters for TCs adsorption onto Fe_3O_4/ZIF-8-G

			Pseudo-first-order model			Pseudo-second-order model			Intra-particle-diffusion model		
Antibiotic	C_0 (mg L^{-1})	$q_{e(exp)}$[a] (mg g^{-1})	$q_{e(cal)}$ (mg g^{-1})	k_1 (min^{-1})	R^2	$q_{e(cal)}$[b] (mg g^{-1})	$k_2 \times 10^{-4}$ (g mg^{-1} min^{-1})	R^2	$q_{e(cal)}$ (mg g^{-1})	k_1 (min^{-1})	R^2
TC	50	127.91	114.23	1.90	0.7499	122.54	204.9	0.9047	15.20	67.34	0.8043
	100	235.81	213.44	1.05	0.7329	231.91	65.9	0.9073	33.19	105.52	0.8782
	200	382.58	344.83	1.66	0.7534	369.45	63.4	0.9283	45.84	201.06	0.8419
OTC	50	140.85	123.75	1.52	0.7582	134.14	146.8	0.9160	18.29	66.53	0.8389
	100	244.11	225.17	1.46	0.7216	240.79	91.5	0.9035	29.81	129.99	0.8120
	200	565.94	515.23	1.44	0.8121	553.13	37.7	0.9541	70.14	290.97	0.8082
CTC	50	238.73	210.26	1.15	0.7767	219.54	67.8	0.9274	33.41	103.00	0.8452
	100	441.20	398.30	0.98	0.8861	435.45	31.3	0.9773	63.75	187.60	0.8057
	200	608.06	559.13	1.99	0.6961	593.25	49.7	0.9020	66.37	353.16	0.8232

[a,b]Present the experimental and calculated values, respectively.

and 258.40 to 568.18 mg g^{-1} for CTC, which were much higher than previous results for removing tetracyclines in aqueous solution (Petit & Bandosz 2011; Ahmed & Jhung 2014; Liu *et al.* 2017; Peng *et al.* 2018). Table 3 lists Langmuir and Freundlich isotherm parameters at temperatures of 298 K, 308 K and 318 K for TCs adsorption on Fe_3O_4/ZIF-8-G. Compared with the Langmuir model in Table 3 (Figure S11), the Freundlich model (Figure S10) fits the experimental data better, and the correlation coefficient $R^2 > 0.9099$ is higher. In addition, the factor '1/n' in the Freundlich isotherm model can reflect the adsorption intensity (Gupta *et al.* 2005). In the present study, the values of 1/n for TCs on Fe_3O_4/ZIF-8-G at three temperatures were less than 0.5, which indicated that the adsorption was easily processed. The values of 1/n were smaller than 0.5.

To further understand the impact of temperature on the adsorption mechanism, the adsorption equilibrium constant (K), free energy change (ΔG, kJ mol^{-1}), enthalpy change (ΔH, kJ mol^{-1}) and entropy change (ΔS, J mol^{-1} K^{-1}) for the TCs adsorption were calculated based on Equations (9) and (10).

As shown in Table S1, the thermodynamic properties for the adsorption of TC, OTC and CTC were calculated from the plot of log (q_e/C_e) vs. $1/T$ (Figure S12), using 100 mg L^{-1} effluent samples at three different temperatures (298 K, 308 K and 318 K). Good linearity with a high regression coefficient for TC, OTC and CTC were obtained.

The values of ΔG were negative at all experimental temperatures. This indicates that the adsorption process of TCs for Fe_3O_4/ZIF-8-G was spontaneous and thermodynamically favorable. The calculated values of ΔH for TCs were 26.81, 87.50, 19.41 kJ mol^{-1}. This may be attributed to the adsorption of TCs onto Fe_3O_4/ZIF-8-G being a physico-chemical adsorption process rather than a pure physisorption or chemisorption process (Arivoli *et al.* 2008; Jain *et al.* 2010). The positive values of ΔS showed an increased randomness at the adsorbent-adsorbate interaction. In conclusion, raising the temperature is beneficial to TCs adsorption on Fe_3O_4/ZIF-8-G.

Comparison with other adsorbents for the adsorption of TCs

To show the advantages of Fe_3O_4/ZIF-8-G for TCs adsorption, the adsorption tests of TCs on ZIF-8, ZIF-8-G, Fe_3O_4/ZIF-8-G, Fe_3O_4/ZIF-8 and Fe_3O_4 were evaluated. As shown in Figure S13, ZIF-8-based materials, except Fe_3O_4/ZIF-8, have excellent removal efficiency for TCs in the initial concentration of 50 mg L^{-1}. However, at a high TCs concentration (200 mg L^{-1}), the efficiency of ZIF-8 decreased below 50% of the original value, while Fe_3O_4/ZIF-8-G still removed up to 90% within 10 h. This indicates that the composite material has a better adsorption capacity than the original ZIF-8 alone.

To show the advantage of Fe_3O_4/ZIF-8-G for the adsorption of TCs, the time-dependent adsorption of TCs on some previously reported methods were evaluated for comparison. The results in Table 4 show that the Fe_3O_4/ZIF-8-G provided a total maximum adsorption capacity up to 1,287 mg·g^{-1} for TC, CTC and OTC in a variety of wastewaters higher than ZIF-8-based other adsorption materials.

Regeneration of Fe_3O_4-ZIF-8/G

The regeneration and convenient recycling of adsorbents are important to green chemistry and practical application. In this work, methanol and acetonitrile, as well as 0.1%

Table 3 | Adsorption isotherm parameters for TCs adsorption onto Fe_3O_4/ZIF-8-G

	Langmuir parameters				Freundlich parameters		
Antibiotic	T(K)	R^2	q_m (mg g^{-1})	b (L mol^{-1})	R^2	K_F	1/n
TC	298	0.9855	159.74	0.105	0.9683	27.41	0.36
	308	0.8727	361.01	0.039	0.9814	9.58	0.40
	318	0.7061	381.68	0.037	0.9723	9.38	0.41
OTC	298	0.9082	198.81	0.043	0.9099	18.58	0.46
	308	0.6972	518.13	0.023	0.9862	22.95	0.39
	318	0.8038	892.86	0.027	0.9798	29.29	0.32
CTC	298	0.9939	258.40	0.538	0.9458	64.32	0.33
	308	0.9932	473.93	0.284	0.9725	86.84	0.42
	318	0.9448	568.18	0.119	0.9701	84.06	0.42

Table 4 | The comparisons of studies on tetracycline antibiotic adsorption on Fe_3O_4/ZIF-8-G and ZIF-based literatures

Material	Specific surface area ($m^2\ g^{-1}$)	Tetracycline species	q_e ($mg\ g^{-1}$)	Temp. (K)/pH	Function	Sample	Reference
ZIF – 8	1295.55	TC	124.6	298/5.0	Absorption	Aqueous solution	Wu *et al.* (2015)
Fe_3O_4@ZIF – 8	1081	TC, OTC, CTC	402.4,-, -	298/4 – 9	Extraction	Anvironmental	Liu *et al.* (2017)
ZIF – 8-ZHC	808.56	TC, NFO, OFO	267.3, 125.6, 227.8	–	Absorption	Water	Tang *et al.* (2019)
ZIF – 8/PDA/PAN fibers	319.38	TC	478.18	298/5	Absorption	Water	Chao *et al.* (2019)
mZIF – 8	1158.2	TC and OTC	303.0, 312.5	303/6.0	Absorption	Wastewater	Li *et al.* (2018)
ZIF – 8	705	CP, TC	29.1, 277.8	–	Absorption	Water	Chen *et al.* (2019)
Fe_3O_4/ZIF – 8-G	509.38	TC, OTC, CTC	238.7, 441.2, 608.0	308/5 – 6	Absorption	Effluent influent aeration water	This method

acetic acid methanol and 0.1% acetic acid acetonitrile solution, were employed to desorb TCs from Fe_3O_4/ZIF-8-G. The results showed that efficient recycling was obtained from washing Fe_3O_4/ZIF-8-G with 0.1% acetic acid methanol solution (v/v) after adsorption (Figure S14).

No significant change in the adsorption capacity for CTC and slight loss for TC and OTC on the regenerated Fe_3O_4/ZIF-8-G were observed after five times reuse (Figure S15). This showed the excellent reusability of Fe_3O_4/ZIF-8-G for the adsorption of TCs in aqueous solution.

Adsorption kinetics of TCs in real wastewater on Fe_3O_4/ZIF-8-G

Three types of wastewater treated spiked samples (100 mL) with three concentration (50 mg L^{-1}, 100 mg L^{-1} and 200 mg L^{-1}) including influent water, aeration water and effluent water from wastewater treatment system. The adsorption kinetics of TCs in three types of wastewater treated spiked samples on Fe_3O_4/ZIF-8-G were evaluated to illustrate the feasibility of Fe_3O_4/ZIF-8-G for practical adsorption of TCs in real wastewater, as shown in Figure S16. All samples obtained were analyzed using HPLC-MS, and calculated by matrix matching standard plots of TCs in three replicates, and the detailed results are outlined in Table 5. There are no significant differences in the adsorption capacity for Fe_3O_4/ZIF-8-G to adsorb TCs from influent water, aeration water and effluent water of wastewater treatment systems. Results showed that Fe_3O_4/ZIF-8-G is a potential material for practical removal of TCs in environmental water.

Table 5 | Adsorption capacity for TC, OTC and CTC onto Fe_3O_4-ZIF-8/G in wastewater samples

		q_e ($mg\ g^{-1}$)		
Antibiotic	Spiked sample	50 mg L^{-1}	100 mg L^{-1}	200 mg L^{-1}
TC	Influent	122.7	247.7	360.2
	Aeration water	122.0	215.2	354.3
	Effluent	122.6	236.1	357.0
OTC	Influent	138.7	220.2	484.3
	Aeration water	147. 2	224.3	483.0
	Effluent	160.7	223.4	485.8
CTC	Influent	245.8	449.7	582.8
	Aeration water	231.6	449.5	583.2
	Effluent	244.1	448.8	581.8

However, due to the complexity of the sewage sample, the target analytes (TCs) were confirmed by mass spectrometry based on the ion ratios and retention time deviations in accordance with the Commission Decision 657/2002/EC. Using HPLC-MS analytical method under optimal absorption experimental conditions, the TC, OTC and CTC were identified and determined in real spiked samples (TC: $t_R = 14.48$ min, $m/z = 445.44$, OTC: $t_R = 15.01$ min, $m/z = 461.44$, CTC: $t_R = 21.6$ min, $m/z = 479.88$). Figure 8 shows the total ion chromatogram of each compound of direct injection after Fe_3O_4/ZIF-8-G-based absorption removal.

CONCLUSIONS

Water-resistant magnetic graphene-anchored zeolite imidazolate (Fe_3O_4/ZIF-8-G) composite materials with the

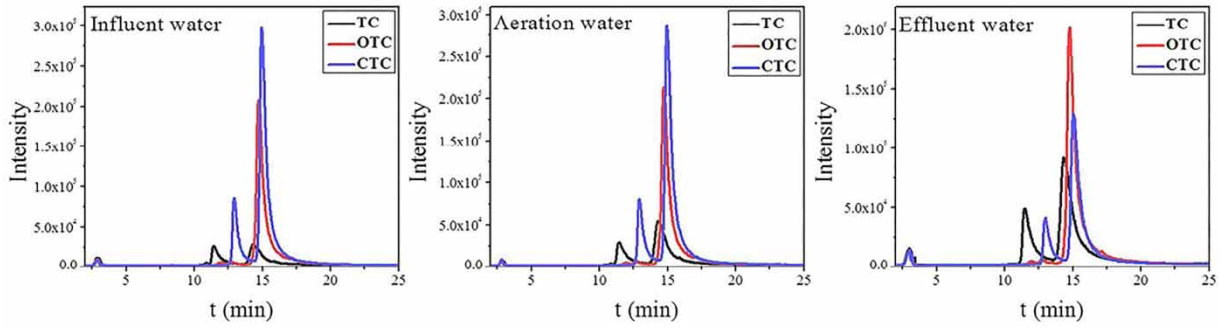

Figure 8 | Chromatogram of direct injection and after Fe_3O_4/ZIF-8-G-based absorption removal for spiking wastewater (100 mg L^{-1}) including influent water, aeration water and effluent water under optimal adsorption conditions ($w = 20$ mg, pH = 5-6, $T = 308$ K).

largest surface area are formed by directly growing a hydrophobic ZIF-8 skeleton onto a graphene support through self-assembly in methanol. Under optimal adsorption conditions, Fe_3O_4/ZIF-8-G hybrid composites with water resistant and super adsorption capacity as an efficient adsorbent for the adsorption and removal of TCs in aqueous solutions were 96.5%, 97.4% and 99.6% within 10 h. Kinetic studies showed that the removal of TCs by Fe_3O_4/ZIF-8-G was a pseudo-second-order reaction. The adsorption process fits the Freundlich isotherm well. The maximum multilayer adsorption capacities of TCs were 382.58 mg g^{-1}, 565.94 mg g^{-1} and 608.06 mg g^{-1} at 308 K, respectively. There is no significant difference in the adsorption kinetics and adsorption capacity for Fe_3O_4/ZIF-8-G to adsorb TCs in pure water or in influent and effluent water. The result indicates that Fe_3O_4/ZIF-8-G is a potential candidate for the removal of mixed antibiotics in wastewater treatment systems.

ACKNOWLEDGEMENTS

We thank the financial support from the National Natural Science Foundation of China (No. 21966024) and (No. 21768003), the National First-Rate Discipline Construction Project of Ningxia (No. NXYLXK2017A04) and the Major Innovations Project for Building First-Class Universities in China's Western Region (No. ZKZD2017003).

SUPPLEMENTARY MATERIAL

The Supplementary Material for this paper is available online at https://dx.doi.org/10.2166/wst.2020.283.

REFERENCES

Ahamad, T., Ruksana, Chaudhary, A. A., Naushad, M. & Alshehri, S. M. 2019 Fabrication of $MnFe_2O_4$ nanoparticles embedded chitosan-diphenylureaformaldehyde resin for the removal of tetracycline from aqueous solution. *Int. J. Biol. Macromol.* **134**, 180–188.

Ahmadi, M., Motlagh, H. R., Jaafarzadeh, N., Mostoufi, A., Saeedi, R., Barzegar, G. & Jorfi, S. 2017 Enhanced photocatalytic degradation of tetracycline and real pharmaceutical wastewater using MWCNT/TiO_2 nano-composite. *J. Environ. Manage.* **186**, 55–63.

Ahmed, I. & Jhung, S. H. 2014 Composites of metal-organic frameworks: preparation and application in adsorption. *Mater. Today* **17**, 136–146.

Ahmed, I., Bhadra, B. N., Lee, H. J. & Jhung, S. H. 2017 Metal-organic framework-derived carbons: preparation from ZIF-8 and application in the adsorptive removal of sulfamethoxazole from water. *Catal. Today* **301**, 90–97.

Arivoli, S., Hema, M., Karuppaiah, M. & Saravanan, S. 2008 Adsorption of chromium ion by acid activated low cost carbon-kinetic, mechanistic, thermodynamic and equilibrium studies. *E-J. Chem.* **5**, 820–831.

Chao, S., Li, X., Li, Y., Wang, Y. & Wang, C. 2019 Preparation of polydopamine-modified zeolitic imidazolate framework-8 functionalized electrospun fibers for efficient removal of tetracycline. *J. Colloid Interface Sci.* **552**, 506–516.

Chen, X., Jiang, X., Yin, C., Zhang, B. & Zhang, Q. 2019 Facile fabrication of hierarchical porous ZIF-8 for enhanced adsorption of antibiotics. *J. Hazard. Mater.* **367**, 194–204.

Chibani, S., Badawi, M., Loiseau, T., Volkringer, C., Cantrel, L. & Paul, J. F. 2018 A DFT study of RuO_4 interaction with porous materials: metal-organic framework (MOFs) and zeolites. *Phys. Chem. Chem. Phys.* **20**, 16770–16776.

El Qada, E. N., Allen, S. J. & Walker, G. M. 2008 Adsorption of basic dyes from aqueous solution onto activated carbons. *Chem. Eng. J.* **135**, 174–184.

Furukawa, H., Cordova, K. E., O'Keeffe, M. & Yaghi, O. M. 2013 The chemistry and applications of metal-organic frameworks. *Science* **341**, 974–986.

Guan, W. H., Gao, X. C., Ji, G. F., Xing, Y. X., Du, C. F. & Liu, Z. L. 2017 Fabrication of a magnetic nanocomposite photocatalysts

Fe_3O_4@ZIF-67 for degradation of dyes in water under visible light irradiation. *J. Solid State Chem.* **255**, 150–156.

Gupta, V. K., Mittal, A. & Gajbe, V. 2005 Adsorption and desorption studies of a water soluble dye, quinoline yellow, using waste materials. *J. Colloid Interface Sci.* **284**, 89–98.

Ho, Y. S. 2006 Review of second-order models for adsorption systems. *J. Hazard. Mater.* **136**, 681–689.

Ho, Y. S. & McKay, G. 1999 Pseudo-second order model for sorption processes. *Process Biochem.* **34**, 451–465.

Islam, G. M. & Gilbride, K. A. 2019 The effect of tetracycline on the structure of the bacterial community in a wastewater treatment system and its effects on nitrogen removal. *J. Hazard. Mater.* **371**, 130–137.

Jain, R., Gupta, V. K. & Sikarwar, S. 2010 Adsorption and desorption studies on hazardous dye naphthol yellow S. *J. Hazard. Mater.* **182**, 749–756.

Jiang, J. Q., Yang, C. X. & Yan, X. P. 2013 Zeolitic imidazolate framework-8 for fast adsorption and removal of benzotriazoles from aqueous solution. *ACS Appl. Mater. Inter.* **5**, 9837–9842.

Jin, J. H., Yang, Z. H., Xiong, W. P., Zhou, Y. Y., Xu, R., Zhang, Y. R., Cao, J., Li, X. & Zhou, C. Y. 2019 Cu and Co nanoparticles co-doped MIL-101 as a novel adsorbent for efficient removal of tetracycline from aqueous solutions. *Sci. Total Environ.* **650**, 408–418.

Kulkarni, A. N., Kadam, A. A., Kachole, M. S. & Govindwar, S. P. 2014 Lichen *Permelia perlata*: a novel system for biodegradation and detoxification of disperse dye solvent red 24. *J. Hazard. Mater.* **276**, 461–468.

Lee, J. W., Choi, S. P., Thiruvenkatachari, R., Shim, W. G. & Moon, H. 2006 Submerged microfiltration membrane coupled with alum coagulation/powdered activated carbon adsorption for complete decolorization of reactive dyes. *Water Res.* **40**, 435–444.

Li, Z., Sun, Q. & Gao, M. Y. 2005 Preparation of water-soluble magnetite nanocrystals from hydrated ferric salts in 2-pyrrolidone: mechanism leading to Fe_3O_4. *Angew. Chem. Int. Ed.* **44**, 123–126.

Li, S., Zhang, X. & Huang, Y. 2017a Zeolitic imidazolate framework-8 derived nanoporous carbon as an effective and recyclable adsorbent for removal of ciprofloxacin antibiotics from water. *J. Hazard. Mater.* **321**, 711–719.

Li, H. Q., Hu, J. T., Meng, Y., Su, J. H. & Wang, X. J. 2017b An investigation into the rapid removal of tetracycline using multilayered graphene-phase biochar derived from waste chicken feather. *Sci. Total Environ.* **603–604**, 39–48.

Li, N., Zhou, L., Jin, X., Owens, G. & Chen, Z. 2018 Simultaneous removal of tetracycline and oxytetracycline antibiotics from wastewater using a ZIF-8 metal organic-framework. *J. Hazard. Mater.* **366**, 563–572.

Liu, H. C., Chen, L. G. & Ding, J. 2017 A core-shell magnetic metal organic framework of type Fe_3O_4@ZIF-8 for the extraction of tetracycline antibiotics from water samples followed by ultra-HPLC-MS analysis. *Microchim Acta.* **184**, 4091–4098.

Mahanta, D., Madras, G., Radhakrishnan, S. & Patil, S. 2008 Adsorption of sulfonated dyes by polyaniline emeraldine salt and its kinetics. *J. Phys. Chem. B.* **112**, 10153–10157.

Mirsoleimani-azizi, S. M., Setoodeh, P., Zeinali, S. & Rahimpour, M. R. 2018 Tetracycline antibiotic removal from aqueous solutions by MOF-5: adsorption isotherm, kinetic and thermodynamic studies. *J. Environ. Chem. Eng.* **6**, 6118–6130.

Özcan, A., Öncü, E. M. & Özcan, A. S. 2005 Kinetics, isotherm and thermodynamic studies of adsorption of acid blue 193 from aqueous solutions onto natural sepiolite. *Colloid. Surface A.* **277**, 90–97.

Peng, Y. G., Zhang, Y. X., Huang, H. L. & Zhong, C. L. 2017 Flexibility induced high-performance MOF-based adsorbent for nitroimidazole antibiotics capture. *Chem. Eng. J.* **333**, 678–685.

Peng, J., Tian, H. R., Du, Q. Z., Hui, X. H. & He, H. 2018 A regenerable sorbent composed of a zeolite imidazolate framework (ZIF-8), Fe_3O_4 and graphene oxide for enrichment of atorvastatin and simvastatin prior to their determination by HPLC. *Microchim. Acta* **185**, 141–150.

Petit, C. & Bandosz, T. J. 2011 Synthesis, characterization, and ammonia adsorption properties of mesoporous metal-organic framework (MIL(Fe))-graphite oxide composites: exploring the limits of materials fabrication. *Adv. Funct. Mater.* **21**, 2108–2117.

Sava, D. F., Chapman, K. W., Rodriguez, M. A., Greathouse, J. A., Crozier, P. S., Zhao, H., Chupas, P. J. & Nenoff, T. M. 2013 Competitive I_2 sorption by Cu-BTC from humid gas streams. *Chem. Mater.* **25**, 2591–2596.

Senta, I., Terzic, S. & Ahel, M. 2013 Occurrence and fate of dissolved and particulate antimicrobials in municipal wastewater treatment. *Water Res.* **47**, 705–714.

Shi, B. Y., Li, G. H., Wang, D. S., Feng, C. H. & Tang, H. X. 2007 Removal of direct dyes by coagulation: the performance of preformed polymeric aluminum species. *J. Hazard. Mater.* **143**, 567–574.

Sumida, K., Rogow, D. L., Mason, J. A., McDonald, T. M., Bloch, E. D., Herm, Z. R., Bae, T. H. & Long, J. R. 2012 Carbon dioxide capture in metal-organic frameworks. *Chem. Rev.* **112**, 724–781.

Tang, H., Li, W., Jiang, H., Lin, R., Wang, Z., Wu, J., He, G., Shearing, P. R. & Brett, D. J. L. 2019 ZIF-8-derived hollow carbon for efficient adsorption of antibiotics. *J. Nanomater.* **9**, 117–126.

Tombuloglu, H., Tombuloglu, G., Slimani, Y., Ercan, I., Sozeri, H. & Baykal, A. 2018 Impact of manganese ferrite ($MnFe_2O_4$) nanoparticles on growth and magnetic character of barley (*Hordeum vulgare* L.). *Environ. Pollut.* **243**, 872–881.

Venna, S. R., Jasinski, J. B. & Carreon, M. A. 2010 Structural evolution of zeolitic imidazolate framework-8. *J. Am. Chem. Soc.* **132**, 18030–18033.

Wang, S. F., Li, X., Liu, Y. G., Zhang, C., Tan, X. F., Zeng, G. M., Song, B. & Jiang, L. H. 2018 Nitrogen-containing amino compounds functionalized graphene oxide: synthesis, characterization and application for the removal of pollutants from wastewater: a review. *J. Hazard. Mater.* **342**, 177–191.

Wu, C. S., Xiong, Z. H., Li, C. & Zhang, J. M. 2015 Zeolitic imidazolate metal organic framework ZIF-8 with ultra-high adsorption capacity bound tetracycline in aqueous solution. *RSC Adv.* **5**, 82127–82137.

Xu, B. B., Wu, F. C., Zhao, X. L. & Liao, H. Q. 2010 Benzotriazole removal from water by Zn-Al-O binary metal oxide adsorbent: behavior, kinetics and mechanism. *J. Hazard. Mater.* **184**, 147–155.

Yang, Z. H., Cao, J., Chen, Y. P., Li, X., Xiong, W. P., Zhou, Y. Y., Zhou, C. Y., Xu, R. & Zhang, Y. R. 2019 Mn-doped zirconium metal-organic framework as an effective adsorbent for removal of tetracycline and Cr(VI) from aqueous solution. *Microporous Mesoporous Mater.* **277**, 277–285.

Yi, M., Shen, Z., Ma, S. & Zhang, X. 2012 A mixed-solvent strategy for facile and green preparation of graphene by liquid-phase exfoliation of graphite. *J Nanopart. Res.* **14**, 1003–1012.

Ying, G. G., He, L. Y., Ying, A. J., Zhang, Q. Q., Liu, Y. S. & Zhao, J. L. 2016 China must reduce its antibiotic use. *Environ. Sci. Technol.* **51**, 1072–1073.

Yoon, M., Srirambalaji, R. & Kim, K. 2012 Homochiral metal-organic frameworks for asymmetric heterogeneous catalysis. *Chem. Rev.* **112**, 1196–1231.

Yu, F., Li, Y., Han, S. & Ma, J. 2016 Adsorptive removal of antibiotics from aqueous solution using carbon materials. *Chemosphere* **153**, 365–385.

Zeng, Z. T., Ye, S. J., Wu, H. P., Xiao, R., Zeng, G. M., Liang, J., Zhang, C., Yu, J. F., Fang, Y. L. & Song, B. 2019 Research on the sustainable efficacy of g-MoS_2 decorated biochar nanocomposites for removing tetracycline hydrochloride from antibiotic-polluted aqueous solution. *Sci. Total Environ.* **648**, 206–217.

Zhang, K., Lively, R. P., Dose, M. E., Brown, A. J., Zhang, C., Chung, J., Nair, S., Koros, W. J. & Chance, R. R. 2013 Alcohol and water adsorption in zeolitic imidazolate frameworks. *Chem. Commun.* **49**, 3245–3247.

Zhang, Q. Q., Ying, G. G., Pan, C. G., Liu, Y. S. & Zhao, J. L. 2015 A comprehensive evaluation of antibiotics emission and fate in the river basins of China: source analysis, multimedia modelling, and linkage to bacterial resistance. *Environ. Sci. Technol.* **49**, 6772–6782.

Zhang, Y. J., Xie, Z. Q., Wang, Z. Q., Feng, X. H., Wang, Y. & Wu, A. G. 2016 Unveiling the adsorption mechanism of zeolitic imidazolate framework-8 with high efficiency for removal of copper ions from aqueous solutions. *Dalton Trans.* **45**, 12653–12660.

Zhao, X. J., Fang, X. L., Wu, B. H., Zheng, L. S. & Zheng, N. F. 2014 Facile synthesis of size-tunable ZIF-8 nanocrystals using reverse micelles as nanoreactors. *Sci. China Chem.* **57**, 141–146.

Zheng, J., Su, C., Zhou, J. W., Xu, L., Qian, Y. Y. & Chen, H. 2017 Effects and mechanisms of ultraviolet, chlorination, and ozone disinfection on antibiotic resistance genes in secondary effluents of municipal wastewater treatment plants. *Chem. Eng. J.* **317**, 309–316.

First received 7 April 2020; accepted in revised form 28 May 2020. Available online 12 June 2020